



ELSEVIER

Available online at www.sciencedirect.com

SCIENCE @ DIRECT®

Journal of Contaminant Hydrology 81 (2005) 34–62

JOURNAL OF

Contaminant
Hydrology

www.elsevier.com/locate/jconhyd

A hybrid method for inverse characterization of subsurface contaminant flux

Mark Newman ^{a,*}, Kirk Hatfield ^a, Joel Hayworth ^b,
P.S.C. Rao ^c, Tom Stauffer ^d

^a *Department of Civil and Coastal Engineering, University of Florida, Gainesville, FL, United States*

^b *Hayworth Engineering Science, Panama City, FL, United States*

^c *School of Civil Engineering, Purdue University, West Lafayette, IN, United States*

^d *Air Force Research Laboratory, Tyndall AFB, FL, United States*

Received 22 March 2004; received in revised form 20 July 2005; accepted 22 July 2005

Available online 31 August 2005

Abstract

The methods presented in this work provide a potential tool for characterizing contaminant source zones in terms of mass flux. The problem was conceptualized by considering contaminant transport through a vertical “flux plane” located between a source zone and a downgradient region where contaminant concentrations were measured. The goal was to develop a robust method capable of providing a statement of the magnitude and uncertainty associated with estimated contaminant mass flux values.

In order to estimate the magnitude and transverse spatial distribution of mass flux through a plane, the problem was considered in an optimization framework. Two numerical optimization techniques were applied, simulated annealing (SA) and minimum relative entropy (MRE). The capabilities of the flux plane model and the numerical solution techniques were evaluated using data from a numerically generated test problem and a nonreactive tracer experiment performed in a three-dimensional aquifer model. Results demonstrate that SA is more robust and converges more quickly than MRE. However, SA is not capable of providing an estimate of the uncertainty associated with the simulated flux values. In contrast, MRE is not as robust as SA, but once in the neighborhood of the optimal solution, it is quite effective as a tool for inferring mass flux probability density functions, expected flux values, and confidence limits.

* Corresponding author. Fax: +1 352 392 3394.

E-mail address: markn@grove.ufl.edu (M. Newman).

A hybrid (SA-MRE) solution technique was developed in order to take advantage of the robust solution capabilities of SA and the uncertainty estimation capabilities of MRE. The coupled technique provided probability density functions and confidence intervals that would not have been available from an independent SA algorithm and they were obtained more efficiently than if provided by an independent MRE algorithm.

© 2005 Elsevier B.V. All rights reserved.

Keywords: Contaminant; Mass flux; Inverse problem; Simulated annealing; Minimum relative entropy; Groundwater

1. Introduction

Groundwater contamination is a worldwide problem and as with any problem of this magnitude the assessment of risk and the appropriate methods for remediation are a constant topic of investigation. However, before risk and remediation can be considered, the task of primary importance is to accurately characterize the source of contamination. The process of source characterization represents solution of an inverse problem and is usually considered within an optimization framework (Gorelick et al., 1983). When posing such a problem, one must consider how to represent or “characterize” the source. A typical practice is to characterize the source by estimating the location and magnitude of contaminant mass within a system. In this construct, risk assessments and remedial actions are based upon estimated contaminant concentrations.

Another option is to characterize the source in terms of mass flux, where flux is a term used to quantify the mass of water and or contaminants flowing through a specified control plane (cross-sectional area) during a given period of time. Based upon this general definition, the units associated with mass flux, m , can be determined as:

$$m = \frac{\text{mass}}{\text{unit area} \cdot \text{time}} = \left[\frac{M}{L^2 \cdot T} \right] \quad (1)$$

where the terms M , L , and T represent the base units of mass, length, and time, respectively. In this framework, risk assessments and remedial actions can be based upon contaminant mass flux. The benefits of flux-based characterization are discussed by Rao et al. (2001).

Regardless of the basis for contaminant source characterization (concentration based or flux based), various optimization methodologies have been applied to the inverse source characterization problem. Gorelick et al. (1983) used least squares regression and linear programming to estimate the magnitude and location of contaminant sources and applied the methods to two hypothetical problems: a steady state leaky pipe problem and a transient contaminant source problem. For the steady state problem, source magnitude was defined as the volumetric flow from each leak in the pipe measured in liters per day [L^3/T], while for the transient case source magnitude was quantified as the mass-loading rate in grams per second [M/T]. Wagner (1992), Aral and Guan (1996), Sidauruk et al. (1998), and Mahar and Datta (2000) and Sciortino et al. (2000, 2002) also presented methods for estimating source magnitude and location. Wagner (1992) used the method

of non-linear maximum likelihood estimation and quantified the source magnitude based upon the mass-loading rate $[M/T]$. Aral and Guan (1996) applied genetic algorithms to estimate source magnitude based upon the contaminant source concentration $[M/L^3]$. Sidauruk et al. (1998) utilized correlation coefficient optimization and applied the method to two-dimensional test problems: one involving an instantaneous point source and the other a continuous point source with the source magnitude being quantified as the mass per unit depth and mass per unit depth per time (2-D mass flux), respectively. Mahar and Datta (2000) applied an embedding technique, which directly incorporated the governing equations for flow and transport into the optimization model. They identified the source magnitude based upon the mass-loading rate $[M/T]$. Sciortino et al. (2000) utilized the Levenberg–Marquardt method to inversely estimate the location and rectangular dimensions of a dense nonaqueous phase liquid (DNAPL) pool located at the base of an aquifer under steady flow conditions. They observed that the inverse model was sensitive to changes in the dispersion coefficients. In later work, Sciortino et al. (2002) applied a genetic algorithm in order to optimize monitoring well networks by minimizing parameter uncertainty along with installation and sampling costs.

Each of these studies conceptualized the source location problem based upon a horizontal discretization of the system and attempted to locate sources by choosing from a discrete set of possible source locations of which the actual source location was a subset. The study that considered the greatest variability of possible solutions was Sciortino et al. (2000, 2002). By considering the location and rectangular dimensions of the contaminant source (DNAPL pool) their model allowed for greater flexibility in characterizing the contaminant source, and by incorporating a random search technique (genetic algorithm) they avoided the limitations of gradient-based optimization methods.

Along with source magnitude and location, Wagner (1992) and Sidauruk et al. (1998) considered source characterization in terms of the transient “disposal history”. Others have also considered the release history and plume evolution problem. Skaggs and Kabala (1994) used Tikhonov regularization to estimate the release history of a simulated one-dimensional contaminant plume. Woodbury and Ulrych (1996) used minimum relative entropy (MRE) to reconstruct plume release and evolution history and applied this method to various one-dimensional test problems including a comparison to Skaggs and Kabala (1994). More recently Woodbury et al. (1998) extended the MRE method to recover the source-release history of a three-dimensional plume produced from a single plane source located at the upgradient boundary of the aquifer system. Atmadja and Bagtzoglou (2001) utilized a hybrid marching-jury backward beam equation and also applied their method to the Skaggs and Kabala (1994) test problem.

McLaughlin et al. (1993) presented a method for site characterization based upon combining field observations with predictions from a stochastic groundwater model. Although, not strictly a “source characterization” approach, this study is included in this review because it provides a concise discussion of the uncertainty associated with contaminant plume characterization. Wagner (1992), Woodbury and Ulrych (1996), and Woodbury et al. (1998) also evaluate the uncertainty associated with estimated source characteristics.

All but three of the previously listed methods were applied solely to numerically simulated test problems. Sciortino et al. (2000, 2002) applied their methods to a

bench-scale dissolution experiment, McLaughlin et al. (1993) applied their methodology to data obtained from a coal tar disposal site in upstate New York; and Woodbury et al. (1998) presented a case study problem at the Gloucester Landfill in Ontario, Canada.

Frind et al. (1999) performed a study specifically for the purpose of investigating the processes involved in field-scale multi-component DNAPL dissolution. They developed a concentration-based numerical model of the Borden emplaced source. The simulation results showed that dissolution and mass transfer at the Borden site occur at or near equilibrium conditions. The work of Frind et al. (1999) demonstrates the conventional method of simulation used for considering contaminant source zones, and the simulation results provide valuable insight into the dissolution process. One thing to note, however, is the amount of prior information that is required for development of the numerical model. In order to simulate the velocity field numerically, a prior estimate of the flow field heterogeneities must exist. For Frind et al. (1999), the flow field was estimated using information from two previous studies (Sudicky, 1989; Woodbury and Sudicky, 1991).

The purpose of the work presented here, as with several of the previously mentioned works, is to characterize contaminant source strength based upon observed contaminant concentration data. The primary difference in this work, when compared to the previous studies, is that here the problem is conceptualized in terms of a vertical flux plane, and the goal is to estimate the spatial distribution and magnitude of contaminant mass flux through the plane. When compared to the conventional method, the primary benefit of the flux plane method is the minimal amount of initial information required for application. In its current form, the flux plane method applies an analytical transfer function, which requires minimal initial information. It is acknowledged that incorporating a numerical solution rather than an analytical solution could expand the applicability of the flux plane model. But development and implementation of a numerical model requires a greater amount of prior information, and such information is not always readily available. By reducing the amount of requisite information the flux plane method provides a simple tool that can be used for preliminary assessment of a contaminant site when very little information is typically known about the flow field and source characteristics. For most preliminary site assessments, all that may be known is the general direction of groundwater flow and the locations of observed downgradient contaminant concentrations. It is specifically for cases such as this, where very little is known, that the flux plane model can provide initial estimates for the total contaminant mass being released from a contaminant source zone.

The other unique aspect of this work is the method of solution. A hybrid solution technique was developed in order to take advantage of the robust solution capabilities of simulated annealing (SA) and the uncertainty estimation capabilities of minimum relative entropy (MRE). The coupled technique provides probability density functions and confidence intervals that are not available from an independent SA algorithm, and they are obtained more efficiently than if provided by an independent MRE algorithm. The capabilities of the methods discussed in this paper were assessed through application to both a numerical test problem and data obtained from laboratory aquifer model experiments.

2. Flux plane model

2.1. Conceptual model

The flux plane conceptual model is shown in Fig. 1. It is assumed that groundwater flow is horizontal and uniform, and that a source zone is continuously releasing contaminants that are transported in the direction of the natural groundwater gradient resulting in a dissolved phase plume. It is also assumed that contaminant concentrations can be measured at multiple locations' downgradient of the contaminant source zone, and that a flux plane is located between the contaminant source zone and the downgradient observation locations.

The conceptual model is represented numerically by dividing the flux plane into N rectangular elements each having a flux component m_n (Fig. 1). The total mass flux through the plane is the sum of the N elemental fluxes, and the resulting concentration (C_j) at location j , has a component contributed from each of the elemental fluxes m_n .

$$C_j = \sum_{n=1}^N g_{jn} m_n \tag{2}$$

In Eq. (2) g_{jn} is a transfer function relating the flux (m_n) through element n , to the concentration (C_j) at location j . Eq. (2) can be used to simulate downgradient concentration values for comparison with observed values and is the forward statement of the inverse problem to be solved.

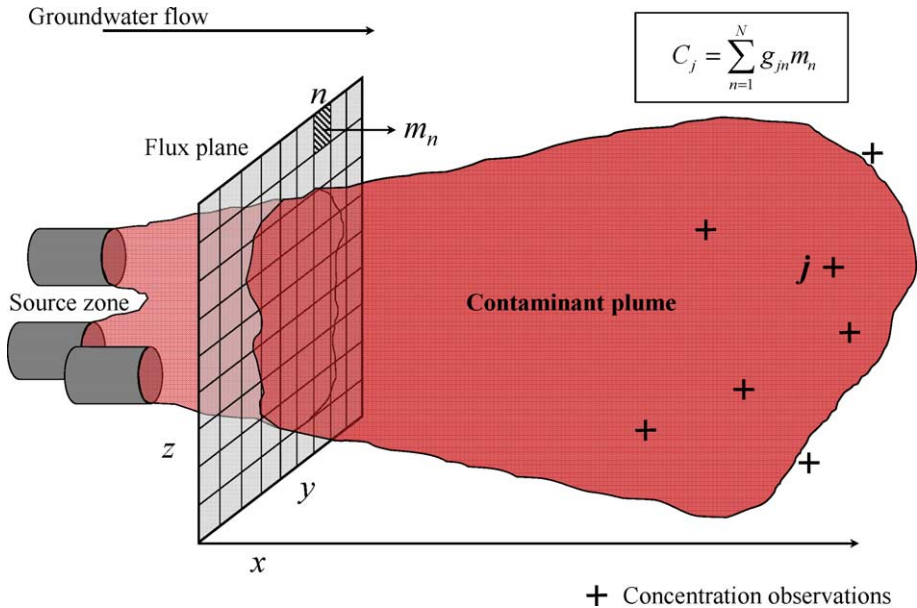


Fig. 1. Flux plane conceptual model.

2.2. Transfer function

With the general forward problem established in Eq. (2), the next step is to determine the form of the transfer function g_{jn} . For this study each of the N flux elements within the flux plane were simulated as a continuous plane source. Domenico and Robbins (1985) presented an analytical solution for three-dimensional transport from a single continuous plane source by solving the equation for advective–dispersive transport in a homogeneous aquifer. The Domenico and Robbins solution is shown below as modified for this investigation.

$$C = \frac{C_o}{8} \operatorname{erfc} \left[\frac{x - vt}{2(\alpha_x vt)} \right] \left\{ \operatorname{erf} \left[\frac{y + b}{2(\alpha_y x)^{1/2}} \right] - \operatorname{erf} \left[\frac{y - b}{2(\alpha_y x)^{1/2}} \right] \right\} \left\{ \operatorname{erf} \left[\frac{z + d}{2(\alpha_z x)^{1/2}} \right] - \operatorname{erf} \left[\frac{z - d}{2(\alpha_z x)^{1/2}} \right] \right\} \quad (3)$$

where erf and erfc represent the error function and complimentary error function respectively. Assuming that the origin for the coordinate axes is located at the center of the plane source, the coordinates x, y, z represent the location of the downgradient concentration C (Fig. 2). The dimensions b and d represent the half-width and half-height of the plane source. C_o is the source concentration [M/L^3], v is the pore water velocity [L/T], t represents the elapsed time [T], and $\alpha_x, \alpha_y, \alpha_z$ represent the dispersivity components along the $x, y,$ and z -axes. The units for $\alpha_x, \alpha_y, \alpha_z$ are length [L].

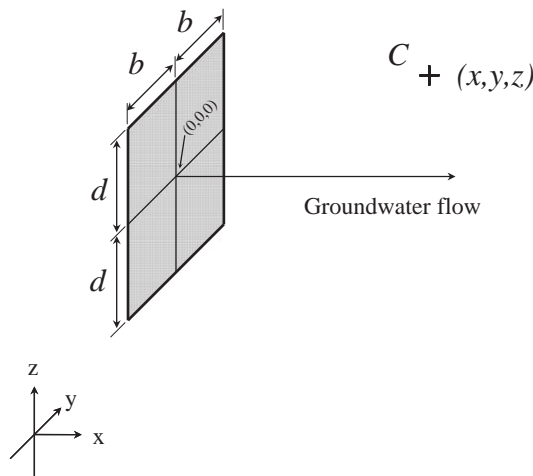


Fig. 2. Schematic of continuous plane source.

Given the analytical solution for three-dimensional transport from a continuous plane source (Eq. (3)) and assuming steady state conditions:

$$\text{As } t \rightarrow \infty; \frac{x - vt}{2(\alpha_x vt)^{1/2}} \rightarrow -\infty; \operatorname{erfc}(-\infty) \rightarrow 2 \quad (4)$$

a transfer function g_{jn} relating the concentration at location j to flux intensity through element n can be formulated as

$$g_{jn} = \frac{1}{4q_x} \left\{ \operatorname{erf} \left[\frac{y'_n + b}{2(\alpha_y x'_n)^{1/2}} \right] - \operatorname{erf} \left[\frac{y'_n - b}{2(\alpha_y x'_n)^{1/2}} \right] \right\} \left\{ \operatorname{erf} \left[\frac{z'_n + d}{2(\alpha_z x'_n)^{1/2}} \right] - \operatorname{erf} \left[\frac{z'_n - d}{2(\alpha_z x'_n)^{1/2}} \right] \right\} \quad (5)$$

where q_x is the specific discharge [L/T] and x'_n, y'_n, z'_n are the relative coordinates defined as

$$\begin{aligned} x'_n &= x_{\text{location } j} - x_{\text{centroid of element } n} \\ y'_n &= y_{\text{location } j} - y_{\text{centroid of element } n} \\ z'_n &= z_{\text{location } j} - z_{\text{centroid of element } n} \end{aligned} \quad (6)$$

Inspection of Eq. (5) shows that the steady state assumption removes the longitudinal dispersivity α_x and velocity v from the transfer function. It should also be noted that there is no retardation term in the transfer function Eq. (5). This indicates that once steady state conditions are achieved the lateral and vertical extents of the plume are determined primarily by the transverse dispersivities α_y and α_z .

With a transfer function defined (Eq. (5)), Eq. (2) can be applied with the objective of determining a set of elemental flux values, m_n ($n=1, 2, \dots, N$), based upon observed concentrations. As mentioned previously, the problem of source characterization is typically solved within an optimization framework (Gorelick et al., 1983). The solution methods applied in this study are discussed in the following section.

3. Numerical solution techniques: nonlinear optimization

Solution of the general problem stated in the previous section requires a nonlinear optimization method capable of dealing with multiple variables. For this study two optimization techniques were investigated, simulated annealing (SA) and minimum relative entropy (MRE). SA was considered due to its robust search capabilities while MRE was considered because of its ability to provide estimates for the probability density function (pdf) of simulated fluxes. The intent was to evaluate the independent capabilities of each method and then consider a hybrid method incorporating the strengths of each.

3.1. Simulated annealing

Simulated annealing is a random search technique. There are a wide variety of random search techniques documented in the literature: simulated annealing, evolutionary algorithms, and neural networks to name a few (Duan et al., 1994; Rogers et al., 1995; Zheng and Wang, 1996; Wang and Zheng, 1998). Each method has its own merits and pitfalls but the above referenced methods all have two similarities: they require only objective function information to determine convergence, so derivative calculations are not required; and they implement probabilistic transition rules, which allow them to avoid local minima in an effort to move towards a global minimum. Typical drawbacks of random search techniques are the computational cost and the fact that although theoretically they should locate a “global” optimum provided adequate time, the reliability of the final estimates are not always readily verified.

The method of simulated annealing (SA), introduced by Kirkpatrick et al. (1983), is an extension of the Metropolis Algorithm (Metropolis et al., 1953), and is based on an analogy with thermodynamics, specifically with the way that metals cool or anneal. The Metropolis algorithm simulates thermal equilibrium at a constant temperature, while SA is a series of Metropolis algorithms evaluated through a sequence of decreasing temperatures.

When applying the thermodynamic analogy to a minimization problem, the energy E of the system for a given temperature represents the objective function value, while the temperature T is an algorithm control parameter which dictates the scale of perturbations and the probability of accepting uphill moves (perturbations that result in increased objective function values). The annealing procedure starts with the system in an initial state that is randomly perturbed. If the resulting change in energy ΔE is negative (the objective function is reduced) then the process is continued in the new state. If the difference in energy is positive (the objective function is increased), the probability of accepting the new state is determined as

$$P = \exp\left[-\frac{\Delta E}{T}\right]. \quad (7)$$

A general SA algorithm is shown in Fig. 3. Laarhoven and Aarts (1987) and Press et al. (1992) provide excellent discussions of the Metropolis algorithm and simulated annealing. For this study, a method of simulated annealing for application with continuous random variables that incorporates the downhill simplex method (Nelder and Mead, 1965) was adapted from Press et al. (1992).

The SA process requires that an annealing schedule be established which controls how and when T is lowered. At higher temperatures, the algorithm creates larger perturbations, and the probability of accepting a move in the direction of higher energy (increased objective function) is greater. As the temperature decreases, the scale of the perturbations decreases, and the probability of accepting moves in the direction of higher energy is reduced. In terms of optimization, this means that at higher temperatures the algorithm is more active—it searches a larger portion of the solution space and is more capable of moving out of local minima. As the temperature decreases the algorithm activity decreases—the search is refined to smaller and smaller portions of the solution space, and the ability to move out of local minima is reduced.

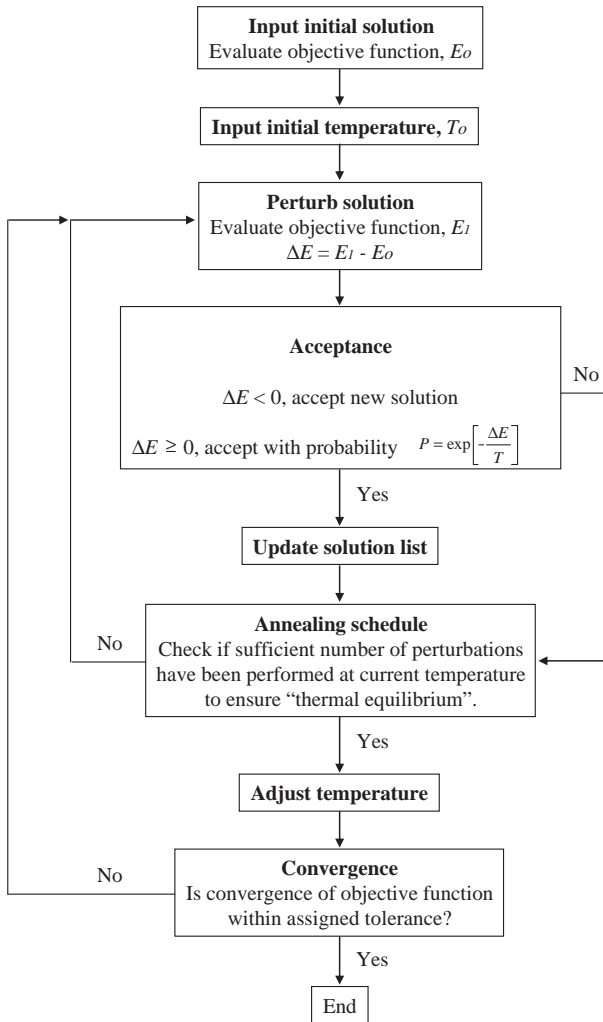


Fig. 3. General simulated annealing (SA) algorithm.

It should be noted that annealing schedules are typically problem specific. An annealing schedule that works well for one system may not be as efficient for another. Press et al. (1992) discuss some possible annealing schedule strategies. For the algorithm applied in this study, the annealing schedule is input as a starting temperature and the maximum number of perturbations to be performed at each temperature increment. As the annealing algorithm is run, the best ever solution (corresponding to the smallest objective function value) is stored for reference along with the $N+1$ previous solutions, where N is the number of unknown variables. The temperature is incrementally decreased by 20% each time the perturbation limit is reached or when all of the $N+1$ solutions differ by the specified convergence criteria. The annealing process continues until the temperature is

reduced to zero (0.00). For this study, application of SA was based upon minimizing the objective function f represented as the sum of the squared differences between observed and simulated concentration values. The problem statement can be summarized as:

$$\text{minimize } f = \sum_{j=1}^M \left(C_{\text{obs},j} - \sum_{n=1}^N g_{jn} m_n \right)^2 \quad (8)$$

$$\text{subject to } m_n \geq L \\ m_n \leq U$$

where M is the number of observations, N is the number of flux elements, $C_{\text{obs},j}$ is the observed concentration value at location j , and $\sum_{n=1}^N g_{jn} m_n$ represents the simulated concentration value at location j (Eq. (2)). L and U represent the lower and upper limits of flux intensity. How values of L and U were assigned for this study is discussed in Section 4.

3.2. Minimum relative entropy

MRE is a gradient-based optimization technique capable of using observation data to infer probability density functions and expected values for unknown model variables. As the term implies, gradient-based optimization techniques are dependent upon calculating the gradient (derivative) of the objective function. Typically, the gradient is used to determine the direction to search for an optimal value. By incorporating gradient calculations, the resulting algorithms are usually very efficient at finding a local minimum when the gradient is steep. But, for cases where the minimum exists in an area with a shallow gradient or where there are numerous local minima, gradient-based methods often have problems converging. Gradient-based methods are usually most efficient once in the general neighborhood of the global optimum.

The term minimal relative entropy is used because the procedure is based upon minimizing the entropy between an unknown pdf and some prior estimate of the pdf. The application of MRE to solve a general linear inverse problem was presented by Woodbury and Ulrych (1996) and was based upon the work of Shore and Johnson (1981). With the application of MRE, portions of the work presented here are an extension of Woodbury and Ulrych (1996) and Woodbury et al. (1998).

Using the notation of Woodbury and Ulrych (1993), \mathbf{x} is an N -dimensional random vector representing one possible state of a system of interest. Next, it is assumed that $q^+(\mathbf{x})$ is the unknown multivariate probability density function (pdf) of \mathbf{x} . When working with continuous random variables, the exact or “true” pdf $q^+(\mathbf{x})$ cannot be directly calculated. However, a posterior estimate $q(\mathbf{x})$ for the true pdf $q^+(\mathbf{x})$ can be established. Within an optimization framework the premise is to minimize the difference between a model simulated (posterior) estimate $q(\mathbf{x})$ and a prior estimate $p(\mathbf{x})$ inferred from observation data.

As with all optimization problems, in order to minimize the difference between observed and simulated values, an efficient method for quantifying the difference has to be established. There are numerous mathematical expressions used to represent the difference between two quantities of interest, one of the simplest being the sum of the squared

differences (which is applied in the SA algorithm). The choice of measure for representing the difference is typically based upon the type of data and the desired result. Relative entropy is a unique measure for comparing observed and simulated values, because it considers the relative uncertainty (Kapur and Kesavan, 1992).

Entropy is a term from the study of thermodynamics that is used to indicate the disorder or randomness of a system. Typically, the symbols S and H are used to represent entropy and enthalpy, respectively. However, for the discussion of relative entropy (or cross-entropy) Shore and Johnson (1981) and Woodbury and Ulrych (1993, 1996, 1998) have consistently defined relative entropy using the symbol H . For the sake of continuity, the same terminology has been applied in this paper.

When applied to optimization, entropy is a measure of the uncertainty involved with the random variables. By minimizing the relative entropy between two pdfs it is assumed that the uncertainty between the pdfs is also reduced (Kapur and Kesavan, 1992). The standard relative entropy equation in terms of q and p is

$$H(q,p) = \int q(\mathbf{x}) \ln \left[\frac{q(\mathbf{x})}{p(\mathbf{x})} \right] d\mathbf{x} \quad (9)$$

where $H(q,p)$ is read as, the entropy of q relative to p . The minimum relative entropy construct leads to a problem statement that differs from that of simulated annealing. In both cases the goal is to “optimize” the contaminant mass flux distribution and magnitude at the flux plane. However, for SA the problem statement is based upon minimizing the sum of the squared differences between observed and simulated values. For MRE the problem statement is represented as

$$\text{Minimize } \int q(\mathbf{x}) \ln \left[\frac{q(\mathbf{x})}{p(\mathbf{x})} \right] d\mathbf{x} \quad (10)$$

$$\text{such that } \int q(\mathbf{x}) d\mathbf{x} = 1 \quad (11)$$

$$\text{and } \int f_j(\mathbf{x}) q(\mathbf{x}) d\mathbf{x} = \bar{f}_j; \quad j = 1, 2, \dots, M \quad (12)$$

where Eq. (11) represents the unity constraint inherent in the definition of a pdf and Eq. (12) represents the expected value constraint. The expected value constraint is developed upon the general relationship for determining the expected value of an arbitrary function, $f_j(\mathbf{x})$. It is assumed that $f_j(\mathbf{x})$ represents a measurable quantity, \bar{f}_j , which represents the observed (mean) value at location j and M is the total number of observations.

The MRE formulation can be solved for the posterior estimate of the pdf (Woodbury and Ulrych, 1993)

$$q(\mathbf{x}) = p(\mathbf{x}) \exp \left[-1 - \mu - \sum_{j=1}^M \lambda_j f_j(\mathbf{x}) \right] \quad (13)$$

where μ and λ_j are Lagrange multipliers. This estimate of the pdf is one of the desirable features of the method of minimum relative entropy. Up to this point, the development has

been in terms of a general variable x . Now, consider a specific set of model variables m . In this case m represents the set of n elemental flux values. To complete the inverse problem the posterior estimate of the pdf $q(m)$ must be used to calculate expected elemental flux values. A method for determining the expected values that is directly applicable to the conceptual problem presented in this paper is that of linear inversion as presented by Woodbury and Ulrych (1996).

Following the linear inversion procedure, the general value for a single observation at point j is (Woodbury and Ulrych, 1996)

$$d_j = \sum_{n=1}^N g_{jn} m_n \quad (14)$$

where d_j represents the observed value at location j , m_n is the model simulated value for the n th flux plane element, g_{jn} is a transfer function relating d_j to m_n , j is the index for the number of observations ($j=1, 2, \dots, M$), and n is the index for the number of flux elements ($n=1, 2, \dots, N$).

Following Woodbury and Ulrych (1996), we can define $q(m)$ as the posterior estimate for the pdf of m :

$$\int_M q(m) \left[\sum_{n=1}^N g_{jn} m_n \right] m = \bar{d}_j \quad (15)$$

Eq. (15) represents the expected or mean observed value \bar{d}_j in terms of the unknown elemental flux values m , the posterior estimate of the pdf $q(m)$, and the transfer functions g .

In order to solve the optimization problem, a set (or vector) of N initial model values S must be established, where each S_n is the corresponding prior estimate of m_n . The resulting expression for S_n is shown below (Woodbury and Ulrych, 1993).

$$S_n = \frac{\exp(-\beta_n U) \beta_n U + \exp(-\beta_n U) - 1}{\beta_n (\exp(-\beta_n U) - 1)} \quad (16)$$

where β_n is a Lagrange multiplier and U is the elemental flux upper limit U .

Applying the prior estimates within the MRE framework, the posterior estimate for the pdf of each individual model m_n can be represented as (Woodbury and Ulrych, 1996)

$$q(m_n) = \frac{-a_n}{\exp(-a_n U) - 1} \exp[-m_n a_n] \quad (17)$$

where a_n is defined as

$$a_n = \beta_n + \sum_{j=1}^M \lambda_j g_{jn} \quad (18)$$

The expected value \bar{m}_n of m_n can then be shown as:

$$\bar{m}_n = \frac{\exp(-a_n U) a_n U + \exp(-a_n U) - 1}{a_n (\exp(-a_n U) - 1)} \quad (19)$$

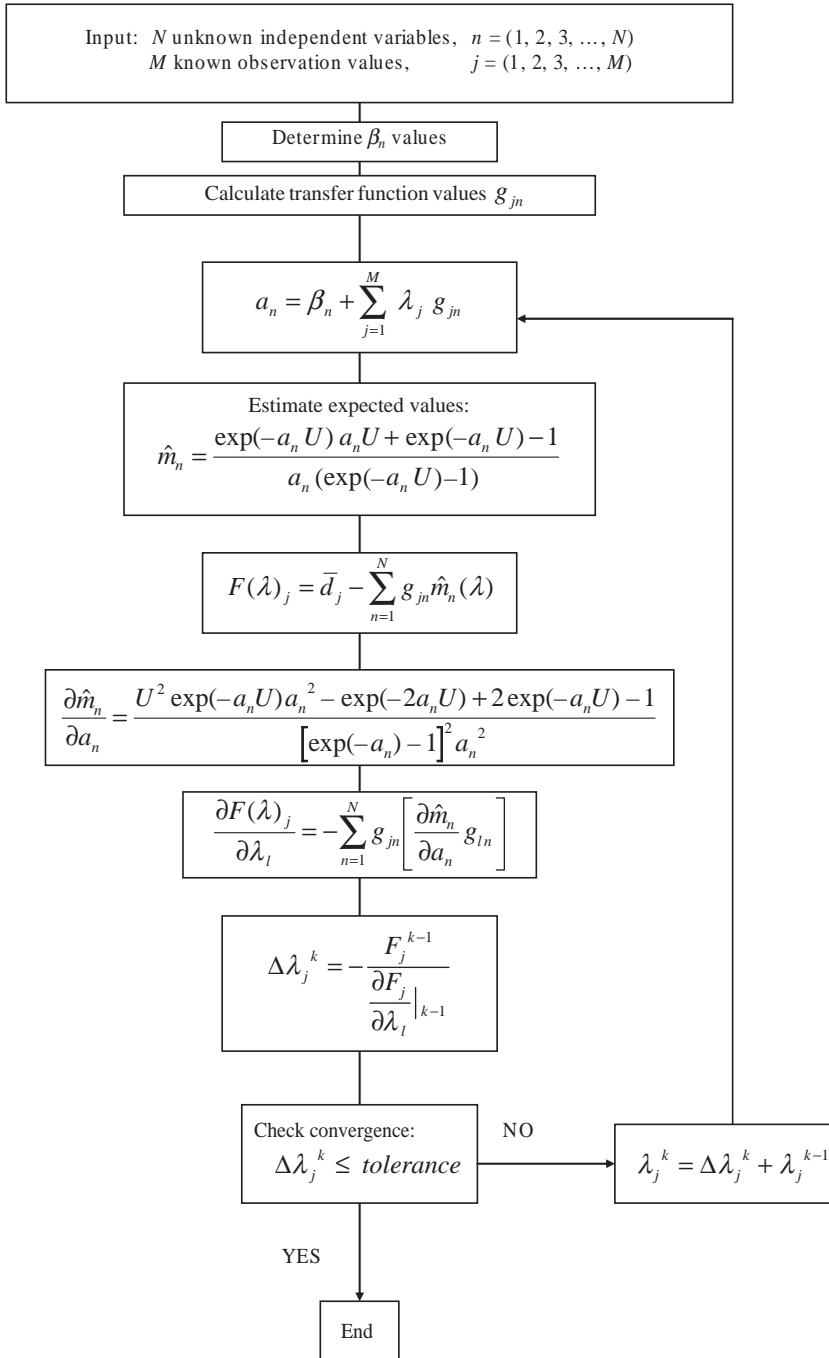


Fig. 4. General minimum relative entropy (MRE) algorithm.

and Eq. (14) can be rewritten as,

$$\bar{d}_j = \sum_{n=1}^N g_{jn} \bar{m}_n \quad (20)$$

Eq. (20) represents the expected (mean) value of the j th observation \bar{d}_j in terms of the transfer function g_{jn} , and expected values of the unknown model parameters \bar{m}_n . Where \bar{m}_n is a function of the Lagrange multipliers β_n and λ_j . It should be noted that Eq. (20) is essentially the same as Eq. (2) used in the development of the conceptual model. The distinction being that Eq. (20) is written explicitly in terms of the expected values of the unknown model parameters (flux) \bar{m}_n , and observed concentration \bar{d}_j .

In order to solve for the expected values (\bar{m}_n) the Lagrange multipliers (β_n) must be determined based upon the prior estimates S_n and the elemental flux upper limit U . Then, the λ_j values are estimated through an iterative procedure that upon convergence results in optimal \bar{m}_n values and posterior estimates of each pdf $q(m_n)$. The general MRE algorithm applied in this study is shown in Fig. 4. Once the algorithm has converged, the final a_n values (based upon optimal λ_j values) can be used to estimate the model parameter confidence intervals. This is done by calculating the individual cumulative density function (cdf) for each model m_n (Woodbury and Ulrych, 1998).

$$P(m_n) = \frac{\exp(-a_n m_n) - 1}{\exp(-a_n U) - 1} \quad 0 \leq m_n \leq U \quad (21)$$

where $P(m_n)$ represents the posterior estimate of the cdf in terms of the Lagrange multipliers (a_n), the parameter upper limit U , and a specified elemental flux value m_n . Solving (Eq. (20)) for m_n yields the following equation,

$$m_n = \frac{\ln[P(\exp[-a_n U] - 1) + 1]}{a_n} \quad (22)$$

which can be used to calculate the elemental flux value corresponding to a specified probability level P .

In order to implement the minimum relative entropy algorithm with the flux plane model presented in this paper, one must first establish the upper limit U for the elemental fluxes. It is important to select a sufficiently large value of U that will allow all expected values of m_n to occur. The value of U can always be lowered once it is determined that none of the simulated m_n values exceed U . It should also be noted that β_n becomes zero and causes a discontinuity when $S_n = U/2$. This should be kept in mind while assigning the initial model values. For this study a modified Powell hybrid algorithm was used to determine the β_n and λ_j values which were then used to estimate expected flux values (m_n).

4. Solution of the flux plane model

Both of the optimization techniques applied in this study have their own unique control parameters. However, there are some parameters common to both methods: the number of

unknowns to be determined, number of observations (amount of prior information), maximum number of iterations, and the convergence tolerance. In order to make an accurate assessment and comparison of each of the methods capabilities, they were applied using a consistent set of control parameters. Both of the methods are capable of determining a feasible solution under certain circumstances, but in order to make a valid comparison it is necessary to answer questions regarding the capability to converge on a feasible solution using the minimal amount of observation data, provide reliable solutions with the least stringent convergence criteria, and comparative computational efficiency. To address these questions, the individual optimization techniques are applied with the flux plane model using data from two cases: a simple numerically generated test problem and a multiple-source tracer experiment performed in a laboratory aquifer model.

4.1. Numerically simulated test problem

The test problem (Fig. 5) represents a simplified version of the intended application of the flux plane model (Fig. 1). A source plane consisting of 49 flux elements was numerically simulated assuming a system specific discharge $q_x=0.5$ m/day, a transverse

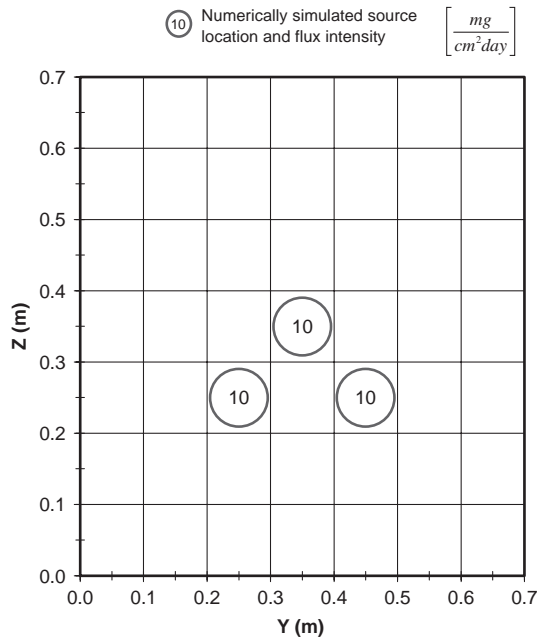


Fig. 5. Numerically simulated flux plane test problem.

System configuration:

- Specific discharge $q=0.5$ m/day
- Transverse dispersivity $a_T=0.0002$ m
- Flux cell half-width $b=0.05$ m
- A total of 24 simulated concentration observations were provided as input (12 observations each at 0.5 m and 1.0 m downgradient of the flux plane).

dispersivity $\alpha_T=0.0002$ m and a square flux element half-width $b=0.05$ m. To create the observation data, three of the flux elements were assumed active with flux intensities of $10 \text{ mg}/(\text{cm}^2 \text{ day})$ and observed downgradient concentrations were simulated at 24 locations (12 each at distances of 0.5 and 1.0 m). The simulated concentration observations were then used as input for the flux plane model. The goal was to use the simulated observations to inversely determine the magnitude and location of the contributing flux elements. As stated earlier, the test problem is an extreme simplification, and was used primarily for algorithm debugging purposes, but it provides a good introduction to the capabilities of the solution techniques.

When implementing the optimization algorithms, each requires a set of initial estimates for the unknown flux elements to be determined. Ideally, input would consist of a uniform initial value over the entire flux plane (as this requires the least amount of prior information), and this was the first approach used. The initial value for each flux cell was set to a flux intensity of $15 \text{ mg}/(\text{cm}^2 \text{ day})$. Using consistent convergence criteria ($1e-04$) and a maximum number of iterations of 1000, SA and MRE were each used to solve the test problem independently. SA was capable of solving the problem by estimating flux intensities of $10 \text{ mg}/(\text{cm}^2 \text{ day})$ for the appropriate elements, and zero everywhere else. MRE reached the maximum number of iterations and did not converge. To verify the robust nature of the SA algorithm, uniform initial values ranging from 0.5 to $50 \text{ mg}/(\text{cm}^2 \text{ day})$ were also used with the test problem, and in each case SA was able to converge on a feasible solution. MRE on the other hand, even with iteration limits in excess of 10,000 and less stringent convergence criteria, was not capable of solving the simple system with a uniform set of initial input values.

However, if sufficient prior information existed such that the set of initial values could be refined, MRE should converge on a feasible solution. For instance, if the set of initial values was segregated into regions of expected high flux values and expected low flux values, MRE should converge more readily. To test this hypothesis, the initial search space was reduced symmetrically around the known location of the sources until the MRE algorithm converged on a solution. It was found that when an initial value of $15 \text{ mg}/(\text{cm}^2 \text{ day})$ was provided for the 20 elements immediately surrounding the known source elements, and a low initial value (between 0 and 1) was provided for the remaining 29 elements, MRE was capable of identifying the three source cells and accurately predicting the flux magnitude for each element to three significant figures. The results indicate that for this simple case, when compared to SA, the initial search space had to be reduced by 60% in order for the MRE algorithm to converge.

It should be noted that the number of iterations performed is not necessarily a suitable comparison for SA and MRE. Because the SA method is based solely upon comparison of objective function values (derivative calculations are not required for each iteration as with MRE), the SA algorithm performs iterations more quickly than MRE. To demonstrate this, the simple test problem was considered without using an early return criterion for the SA algorithm (meaning the algorithm is forced to perform 1000 iterations regardless of when convergence is met). The SA algorithm performed 1000 iterations 15 times faster than MRE and converged on a solution, while MRE took longer and did not converge. For larger problems, such as the laboratory scale problem considered in Section 5, the difference in computational speed is even greater.

The initial applications of MRE and SA with the test problem emphasize one of the primary differences between application of gradient-based (MRE) and random search (SA) methods: when provided a large number of possible solutions random search methods are typically more robust and capable of avoiding local minima in favor of the global minimum, while gradient-based methods are typically most efficient once in the neighborhood of a global minimum.

The primary reason for discussing the test problem was to demonstrate the robust search capabilities of the SA algorithm and to introduce the necessity for segregating the search space for the MRE algorithm. The initial results indicate that a greater amount of prior information is required for the MRE algorithm to converge on a feasible solution. With the test problem, this prior information is readily available, but for application to a real system the amount of prior information is usually limited. One way to minimize the amount of prior information required for MRE to converge is a combined SA-MRE algorithm.

4.2. SA-MRE hybrid method

For the SA-MRE method, SA is used to provide an initial solution based upon minimal prior information (a uniform set of initial values). The SA solution is then passed to the MRE algorithm, which refines the solution while providing a measure of parameter uncertainty. As mentioned previously, random search techniques such as SA are very robust and can typically avoid local minima while converging on the global minimum. However, the reliability of the final solution is not readily verified. This leads to the question, how does one determine if the SA solution is in the neighborhood of the global minimum so that MRE can converge efficiently? For this study, the reliability of the SA solution was estimated by using a multi-leveled annealing schedule. Essentially, three independent annealing processes are performed (each starting with the same initial set of uniform values but with different initial temperatures and perturbation limits). Because each annealing process is random and independent, they provide verification of one another. The minimum objective function value along with the corresponding flux values from each process are stored for comparison, and if all three are within a defined tolerance the best set of flux values (the set with the lowest objective function value) is passed to the MRE algorithm. The set of flux values determined with SA now represent the initial flux values (S_n) for MRE. The S_n values and the upper limit U are used with Eq. (16) to estimate the corresponding β_n values necessary for application of the MRE algorithm. The independent SA and MRE algorithms along with the hybrid SA-MRE method were verified using data from laboratory aquifer experiments.

5. Laboratory aquifer model

The aquifer model used for this study was constructed at the Air Force Research Laboratory, Tyndall Air Force Base, Florida. The system was designed for use with chlorinated solvents; all wetted surfaces were stainless steel or glass, minimizing the

Table 1
Physical, hydraulic, and transport properties of the three-dimensional aquifer model (Newman, 2001)

Parameter	Value
Porous media	Flint Silica #14 (U.S. Silica, Ottawa, IL)
Porous media dimensions (length \times width \times height; m)	$2.0 \times 0.5 \times 1.0$
Median grain size (d_{50} ; m)	0.0012
Porosity (n)	0.3
Longitudinal dispersivity (α_L ; m)	0.001–0.003
Transverse dispersivity (α_T ; m)	0.0002

partitioning of hydrophobic chemicals to system components. All liquid effluent and vapor streams passed through physical and/or chemical traps, eliminating exposure to hazardous chemicals and allowing quantitative mass balance determinations. In the experiments performed for this study, the model was configured to simulate a homogeneous surficial aquifer. The porous medium was a clean, medium grained silica sand (Flint Silica #14). The volumetric flowrate and corresponding pore water velocity were controlled by manipulating the elevations of the inlet and outlet head tanks. The physical, hydrodynamic, and transport characteristics of the system are presented in Table 1. The experimental procedures and numerical analysis used to determine the dispersivities are discussed by Newman (2001). A series of multi-point samplers were emplaced within the flow system providing a three-dimensional distribution of over 500 sampling points within the porous media. The longitudinal distribution (x – z plane) of multi-point samplers is shown in Fig. 6. The lateral distribution (y – z plane) of sample points varies with location along the longitudinal (x) axis. Some transects have a minimum of 20 sample points while

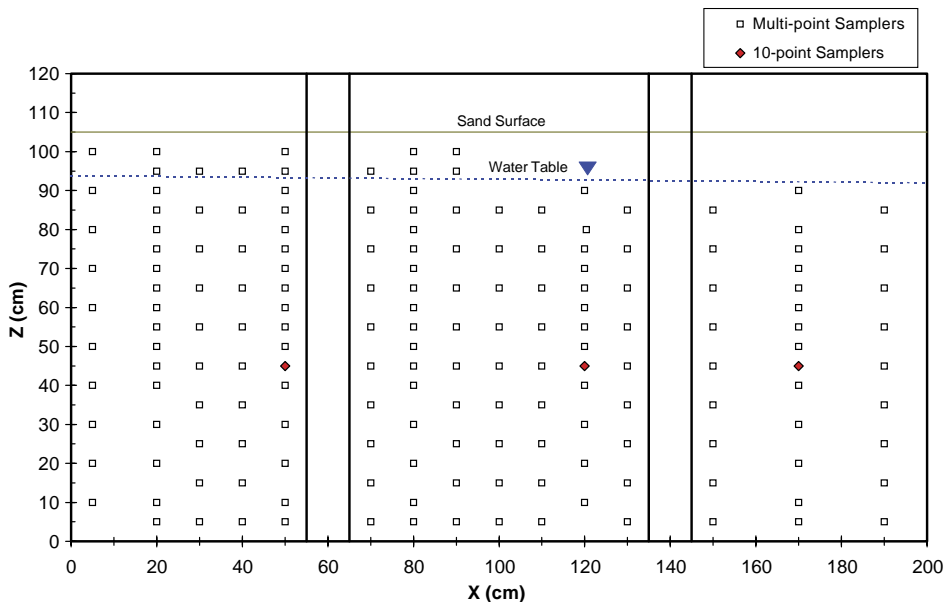


Fig. 6. Schematic of the multi-sampler distribution along a longitudinal transect of the aquifer model.

the more extensive transects have up to 72 sample points. Fig. 7 shows one of the more extensive transects located at $x=0.2$ m, which for this experiment is also the location of the source injection ports.

5.1. Multiple source tracer experiment

The multiple source tracer experiment was started by establishing a steady flow field with an average saturated thickness (h_s) of 0.79 m, and an average pore water velocity of 0.54 m/day (corresponding to a specific discharge of $q=0.161$ m/day). Then, three steady state plumes were developed by continuous injection of bromide (Br^-), chloride (Cl^-), and sulfate (SO_4^{2-}) tracer solutions (200 mg/l each) from three separate injection ports, located within the upgradient, saturated region of the flow system. Experimental conditions including source injection rates, calculated mass loading rates, and system flow parameters are summarized in Table 2. The source locations are shown in Figs. 7 and 8. The motivation for using three different ionic tracers was to provide the ability to distinguish between the contributions of each point source to the combined downgradient plume. Because all three tracers are non-reactive the tracer concentrations were combined and treated as one single contaminant for this analysis. However, the ability to distinguish between the contributions of each source

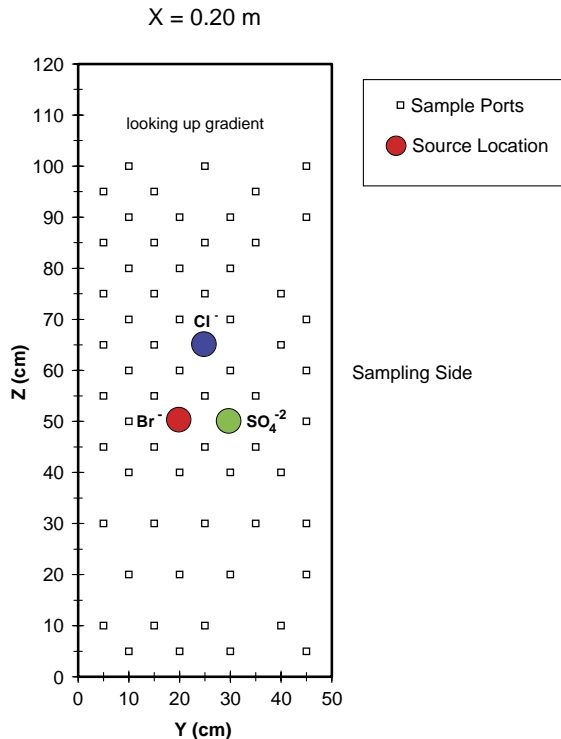


Fig. 7. Source locations (transect $x=0.2$ m) for multiple source tracer experiment.

Table 2
System parameters for the multi-source tracer experiment

Parameter	Value
Source no. 1 (chloride)	
Injection point location (x, y, z ; m)	0.20, 0.25, 0.65
Concentration (mg/l)	200
Injection Rate (ml/min)	0.8
Mass loading rate (mg/day)	230.4
Source no. 2 (bromide)	
Injection point location (x, y, z ; m)	0.20, 0.20, 0.50
Concentration (mg/l)	200
Injection rate (ml/min)	0.378
Mass loading rate (mg/day)	108.9
Source no. 1 (sulfate)	
Injection point location (x, y, z ; m)	0.20, 0.30, 0.50
Concentration (mg/l)	200
Injection rate (ml/min)	0.373
Mass loading rate (mg/day)	107.4
Flow parameters	
Average saturated thickness (h_s ; m)	0.79
Average effluent water flowrate (Q_x ; m ³ /day)	0.0635
Specific discharge (q_x ; m/day)	0.161
Average pore water velocity (v ; m/day)	0.54

allowed for additional scrutiny of the numerical capabilities for estimating the spatial distribution of mass flux. It also provided helpful information for trouble-shooting simulated flux values at zones of plume overlap during the early stages of model verification.

Transient tracer concentrations were measured at multiple locations along the flow path in order to determine when steady state conditions were established. Once the plumes had reached steady state, tracer concentrations were collected throughout the entire model aquifer domain providing a “snap shot” of the steady state tracer distribution within the porous media (Fig. 8). The sources are located at transect $x=0.2$ m and the tracer distributions are shown for transects $x=0.5, 0.8, 1.2,$ and 1.7 m.

5.2. Flux plane model application to laboratory tracer experiment data

The observed tracer concentrations from the multiple-source tracer experiment performed in the laboratory aquifer model (Fig. 8) were used as input to test the ability of each algorithm for estimating mass flux. Five different simulation scenarios were considered (Fig. 9) using the laboratory data. Each scenario represented a different set of “observed” data, which were used to inversely determine the flux magnitude and distribution at the source plane. The purpose for considering the different scenarios was to consider how the number and location of observations affects the inverse flux estimates. In Scenario 1, the measured data from each of the 4 downgradient transects were used as observed data for inversely simulating the mass flux at the source plane. In Scenario 2, the measured data from the furthest two transects ($x=1.2$ and 1.5 m) were

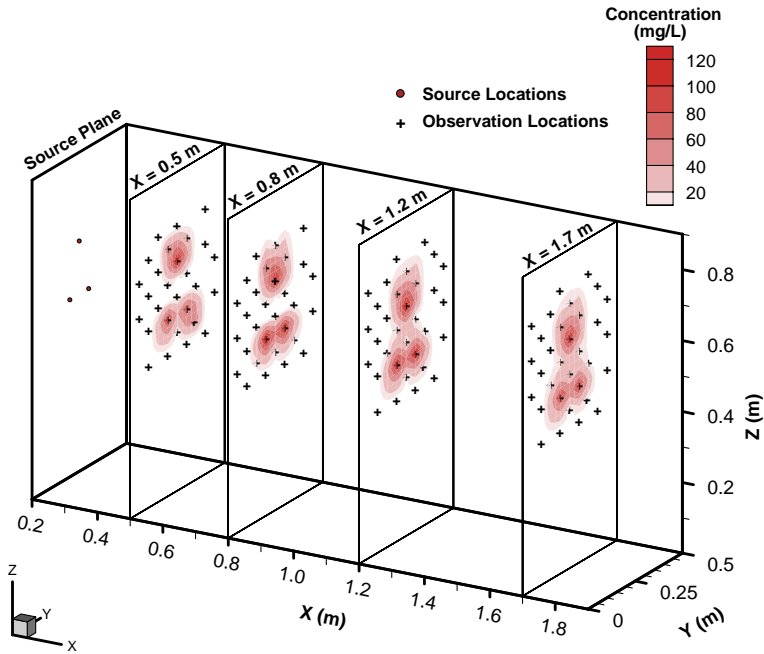


Fig. 8. Steady state three-dimensional tracer distribution for Day 7.

used as observation data to inversely simulate the mass flux at the source plane. The simulated flux values were then used to solve the forward problem and predict resulting tracer concentrations at the two transects ($x=0.5$ and 0.8 m) nearest the flux plane. The predicted concentrations were then compared to the observed concentrations to verify the simulation results. The remaining three scenarios were performed similarly as indicated in Fig. 9.

In order to verify results of the inverse simulations, a method for comparing the model-simulated fluxes to the known tracer injection rates was necessary. To do this, the injection concentration (200 mg/l) for each tracer was used with the source injection rates to estimate mass loading rates at the source plane (Table 2). Then, the mass loading rates were compared to the integrated mass flux values determined from the model-simulated fluxes. The comparison was considered as the percent mass recovered (calculated as the ratio of total simulated mass flux through the plane to the sum of the estimated mass loading rates for each of the tracers).

The flux plane used for application with the multiple source tracer data consisted of 442 elements, each representing a 2-cm square plane source with a possible flux intensity ranging from a lower limit of $0 \text{ mg}/(\text{cm}^2 \text{ day})$ to the specified upper limit U . The upper limit is established based upon the specific discharge ($q=0.161 \text{ m/day}$) and an assumed tracer concentration limit. It was known that the tracers were injected as 200 mg/l solutions so the true flux upper limit is $3.22 \text{ mg}/(\text{cm}^2 \text{ day})$, but for practical application the true upper limit would not be known. A series of simulations were run using values of U ranging from 3.22 to $16.10 \text{ mg}/(\text{cm}^2 \text{ day})$ corresponding to concentration limits of 200 and

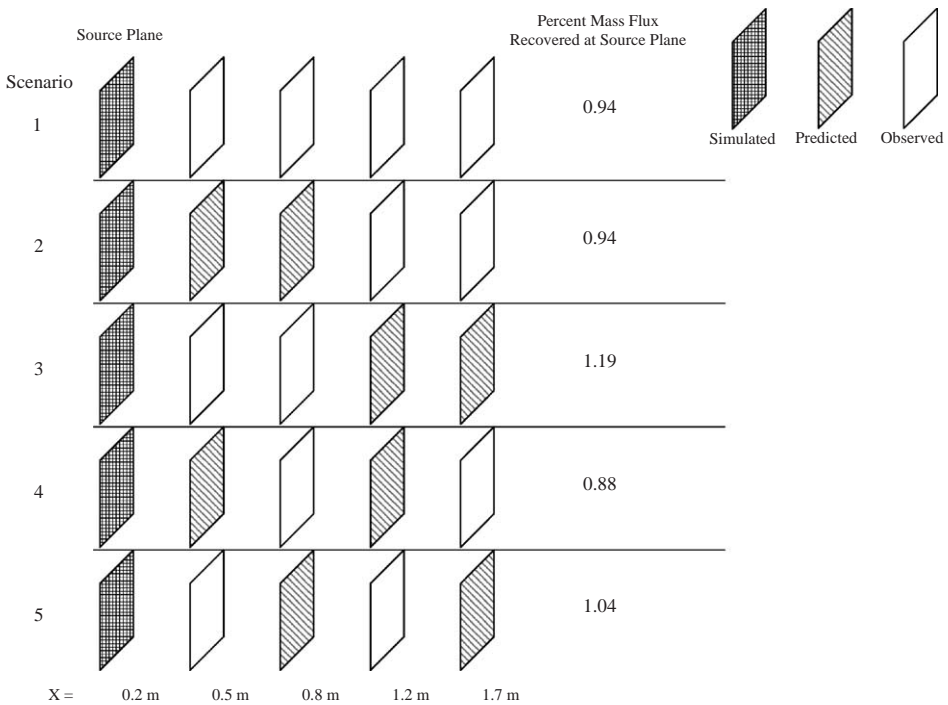


Fig. 9. Simulation scenarios and resulting tracer mass recovery at the source plane.

1000 mg/l, respectively. It was found that the integrated mass flux was not very sensitive to the upper limit, but the spatial distribution of the flux intensities within the flux plane was. As the upper limit increases, the spatial distribution of flux intensities approaches the case where only three flux elements are active (one for each injection point) each with very high flux intensity. It was found that an upper limit of 4.83 mg/(cm² day) (corresponding to a concentration limit of 300 mg/l) provided both consistent integrated mass flux values and spatial distributions.

An order of magnitude sensitivity analysis was performed to evaluate the model sensitivity to transverse dispersion. Results for transverse dispersivity (α_T) values of 0.002, 0.0002, and 0.00002 m were compared for Scenario 1, and the corresponding percent mass recovered at the flux plane was 1.17, 1.07, and 1.04, respectively. This indicates that in terms of the integrated mass flux, the model is not extremely sensitive to transverse dispersion. What does vary between these cases is the distribution of simulated flux intensity within the plane. For the case with higher dispersion, there are smaller zones of high flux intensity, while for the case of lower dispersion there are larger zones of lower flux intensity.

The model sensitivity to U and α_T is directly related to the size of the flux elements. If the plane is discretized such that the elements are smaller than the expected scale of the source zone, the model is allowed greater flexibility when trying to match the integrated mass flux across the plane. The result is that the total flux across the plane and the total contribution of each element to downgradient concentrations is not very sensitive to changes in U and α_T .

The five simulation scenarios were evaluated using SA, MRE, and the hybrid SA-MRE method. As with the numerical test problem, MRE required a greater amount of prior information in order to isolate the source zone and converge on a feasible solution. For this problem the initial search space of 442 flux elements had to be reduced by 64% in order for the MRE algorithm to converge. When the MRE algorithm did converge, the mass recovery for the independent SA and MRE algorithms were practically the same. For the 5 scenarios considered, the MRE result was on average 0.01% less than the SA result. The results demonstrate that the major differences between the two methods are the amount of required prior information and the comparative computational speed. For application with the laboratory aquifer data, SA is by far the faster algorithm, typically converging 50 times faster than MRE.

Application of the hybrid SA-MRE method produced flux values that were similar to those obtained by the independent algorithms. For Scenario 5 the SA, MRE, and SA-MRE percent mass recovered were 1.05, 1.04, and 1.04, respectively. What should be noted is that on average the SA-MRE algorithm converged 10 times faster than MRE. This indicates that the primary distinction between the MRE and SA-MRE methods is not the accuracy of the final results, but the fact that the hybrid method converges faster than the independent MRE algorithm while requiring less prior information.

The percent mass flux recovered at the source plane for each scenario using SA-MRE is shown in Fig. 9. The largest error was seen in Scenario 3, where the integrated mass flux at the source plane was overestimated by 19%. Scenario 5 showed the best mass recovery (1.04), slightly overestimating the integrated mass flux at the source plane by 4%. The corresponding spatial distribution of simulated mass flux for Scenario 5 is shown in Fig. 10.

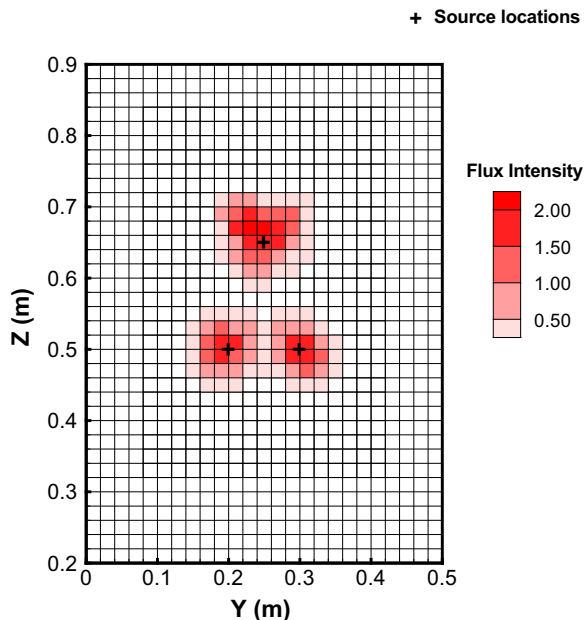


Fig. 10. SA-MRE simulated elemental mass flux distribution at the source plane.

The information available from the aquifer experiments does not allow direct verification of the spatial distribution, however the scale of the source zones were estimated by equating the system specific discharge to the known mass injection rates at each of the three tracer injection locations. For the chloride source (which had the greater injection rate) the estimated width of a square source injection zone was 9 cm. The apparent model simulated width was approximately 12 to 14 cm (Fig. 10). For the bromide and sulfate sources (which had the same injection rates) the estimated width of a square source injection zone was 6 cm and the apparent model simulated width was approximately 8 to 10 cm.

As discussed previously, the primary reason for incorporating MRE in the hybrid method is to provide a measure of the uncertainty related with the simulated flux values. Fig. 11 shows the SA-MRE estimates for the pdf, 95% confidence interval, and mean (expected) value of the mass flux for one of the source plane elements ($y=0.25$ m, $z=0.65$ m), where the initial pdf is the uniform (box car) distribution and the final pdf is the truncated exponential (Eq. (16)) as discussed by Woodbury and Urych (1996). The intermediate pdf is one of many intermediate distributions that are developed while iterating to solve the inverse problem. The SA-MRE algorithm provides similar estimates for each of the 442 flux elements within the flux plane.

To demonstrate the affect of the assigned upper limit U on the model results, the expected flux magnitude and estimated 95% confidence interval for each of the 442 source plane elements were plotted as shown in Figs. 12 and 13. For the case of an upper flux limit of 4.83 mg/cm² day (Fig. 12), it is evident that greater confidence is associated with estimated flux values at either end of the range of simulated expected values. Remembering that the upper limit U is set at 4.83 mg/(cm² day) when it is

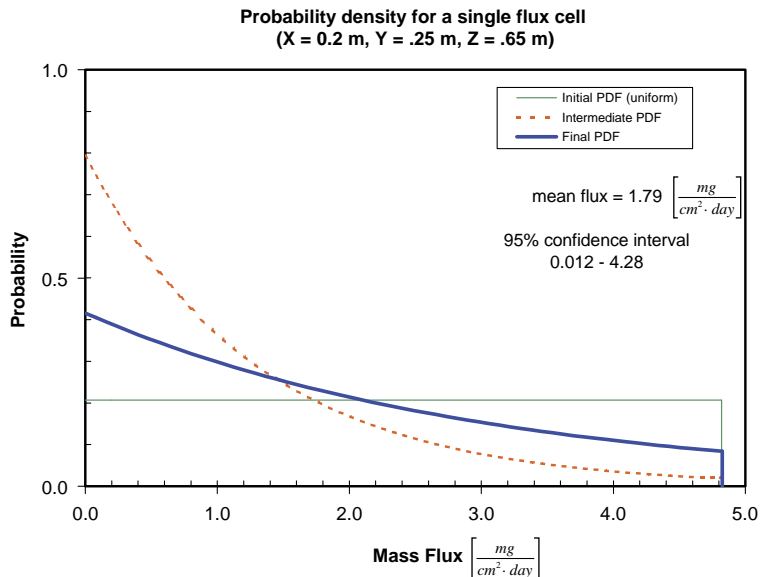


Fig. 11. Estimated probability density function and 95% confidence interval for a single flux cell from the multiple ionic source tracer experiment.

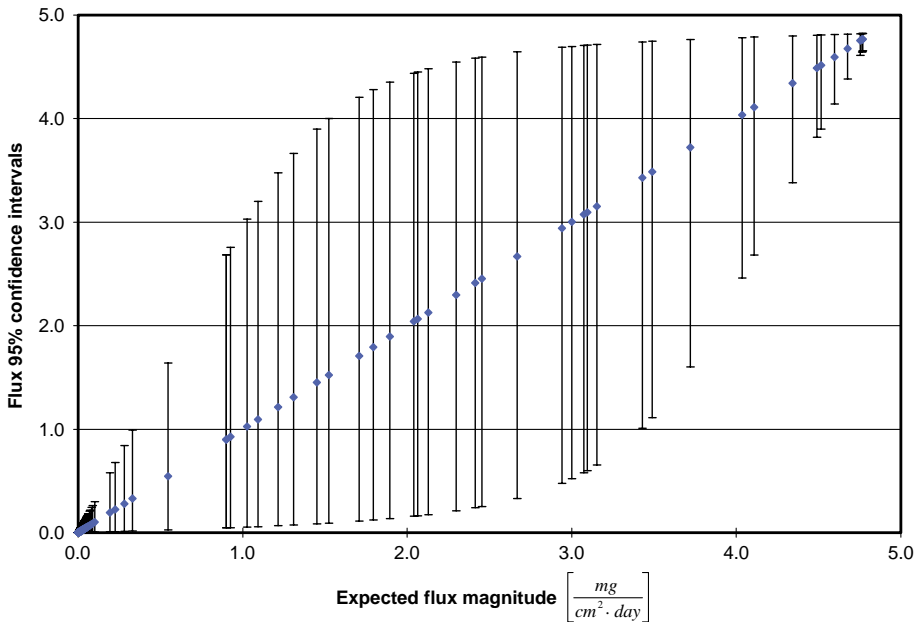


Fig. 12. Estimated 95% confidence intervals for all 442 source plane elements using a flux upper limit of 4.83 (mg/cm^2 day).

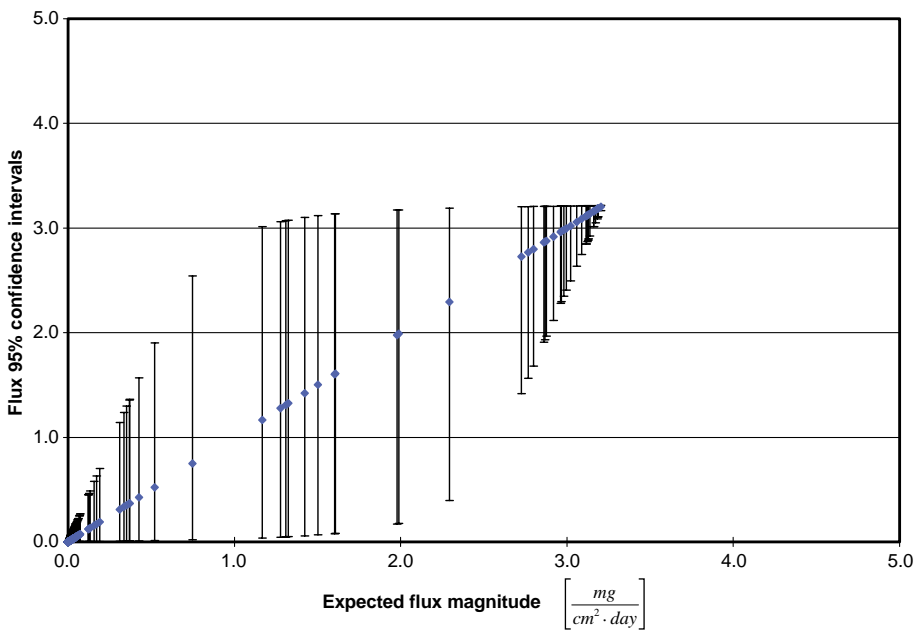


Fig. 13. Estimated 95% confidence intervals for all 442 source plane elements using a flux upper limit of 3.22 (mg/cm^2 day).

known to be approximately $3.22 \text{ mg}/(\text{cm}^2 \text{ day})$ note the smooth distribution of expected flux values within the specified range, while the corresponding confidence intervals are relatively large. If the more informed flux upper limit of $3.22 \text{ mg}/(\text{cm}^2 \text{ day})$ is used (Fig. 13) the distribution of expected values is not as smooth between the upper and lower bound, but the confidence associated with each of the expected flux values is improved. This is expected because with a more stringent upper limit, the model does not have as much freedom to distribute the contribution of flux elements within the source plane. A greater number of flux elements are set closer to the upper and lower bounds and fewer are set at intermediate values. Comparison of Figs. 12 and 13 demonstrates the capability of the hybrid method to incorporate additional prior information in order to update flux estimates and improve the confidence associated with the estimates.

For additional verification of the inverse simulation results, the SA-MRE expected flux values for Scenarios 2 through 5 were used to provide forward predictions of downgradient concentrations as indicated in Fig. 9. Fig. 14 compares the model predicted concentrations to the observed concentrations for Scenario 5 using the less informed flux upper limit of $4.83 \text{ mg}/(\text{cm}^2 \text{ day})$. The maximum absolute error was $29 \text{ mg}/\text{l}$ with an average absolute error of $0.76 \text{ mg}/\text{l}$. The results from Scenario 5 are representative of the predictions obtained for the other scenarios. The forward simulation results demonstrate that the simulated mass flux values at the source plane

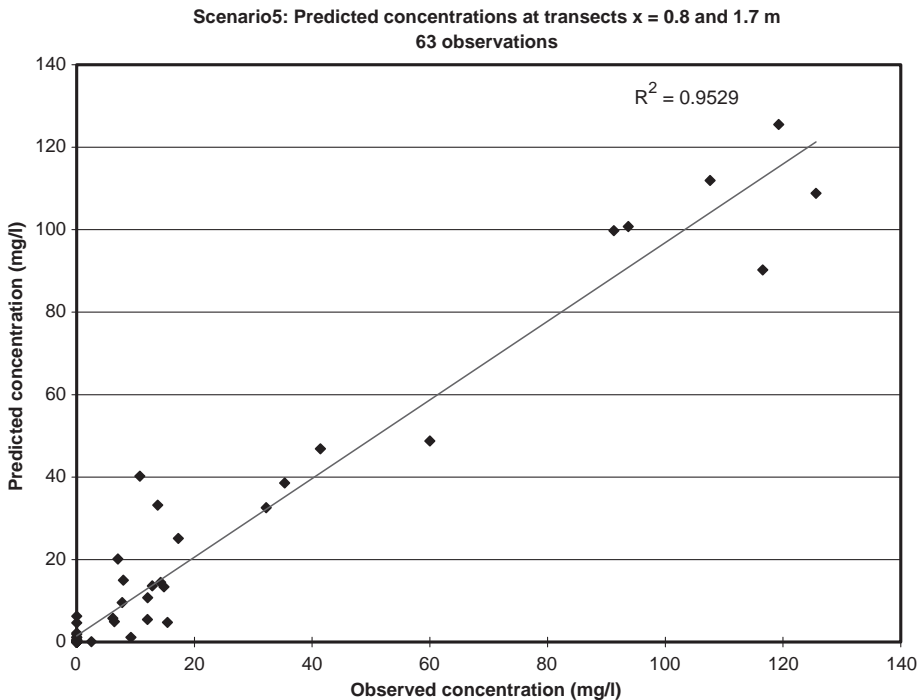


Fig. 14. Plot of observed vs. predicted concentrations for simulation Scenario 5 and upper flux limit of $4.83 \text{ mg}/(\text{cm}^2 \text{ day})$.

can be used to provide reasonable predictions for downgradient contaminant concentrations.

6. Summary and discussion

With the goal of developing a tool for characterizing contaminant source zones in terms of mass flux, a hybrid SA-MRE method was applied in conjunction with a flux plane model. SA-MRE takes advantage of the robust solution capabilities of SA and the uncertainty estimation capabilities of MRE. The coupled technique provides probability density functions and confidence intervals that are not available from an independent SA algorithm and they are obtained more efficiently than if determined by an independent MRE algorithm. SA-MRE along with the flux plane model provides a robust method for estimating contaminant mass flux values and provides a measure of the uncertainty associated with the flux values.

An important characteristic of the flux plane model is the size of the individual elements. Although, the individual flux elements are sensitive to U and α_T , the controlling factor in model convergence is the combined contribution of the flux elements, not the individual flux intensities. If the flux elements are established such that their size is considerably smaller than the expected scale of the contaminant source zone, the effect of individual flux error is reduced.

In its current form, the flux plane model is admittedly a simplification of a more complex problem and is only applicable under the conditions assumed for the applied transfer function (steady state, uniform, horizontal flow in a homogeneous aquifer). It should be noted that incorporating a different transfer function, perhaps a numerical solution rather than an analytical solution, could expand the applicability of the flux plane model by incorporating flow field heterogeneities. However, implementing a numerical solution significantly increases the level of requisite information and this information is not always readily available. In its current form the model provides a simple method for providing initial estimates for the magnitude and spatial distribution of contaminant mass flux based upon observed groundwater contaminant concentrations. For the five simulation scenarios presented in this study, the integrated mass flux ranged from 88% to 119% of the known total flux (Fig. 9).

The simplicity of the flux plane concept allows for relatively quick application of the model, and because the model utilizes average hydrodynamic parameters and bulk hydrogeological property values, the model does not require a large amount of site characterization data. The requisite data represent standard information that is typically obtained during initial site assessments. The flux plane model relates observed contaminant concentrations to mass flux through a plane, and provides a method for estimating the integrated mass flux or total mass crossing a specified boundary. This boundary could represent a regulatory boundary or the intersection of adjoining properties, and the results provide an estimate of the total mass crossing the boundary. The method can be easily modified to incorporate different transfer functions, and would be especially applicable if utilized with directly measured contaminant flux values obtained using a method such as that presented by Hatfield et al., 2004.

Acknowledgements

Portions of this research were funded by the Natural and Accelerated Bioremediation Research (NABR) program, Biological and Environmental Research (BER), U.S. Department of Energy (Grant Number DE-FG02-97ER62471), the Florida Water Resources Center under a grant from the U.S. Department of Interior (Grant Number: 01HQGR0138), and the Environmental Security Technology Certification (ESTCP) program, U.S. Department of Defense (DoD): (Project Number CU-0114). This paper has not been subject to DoD review and accordingly does not necessarily reflect the views of DoD.

References

- Aral, M.M., Guan, J., 1996. Genetic algorithms in search of groundwater pollution sources. In: Aral, M.M. (Ed.), *Advances in Groundwater Pollution Control and Remediation*, NATO ASI series. Kluwer Academic Publishers, Dordrecht, The Netherlands, pp. 347–369.
- Atmadja, J., Bagtzoglou, A.C., 2001. Pollution source identification in heterogeneous porous media. *Water Resour. Res.* 37 (8), 2113–2125.
- Domenico, P.A., Robbins, G.A., 1985. A new method of contaminant plume analysis. *Ground Water* 23 (4), 476–485.
- Duan, Q., Sorooshian, S., Gupta, V.K., 1994. Optimal use of the SCE-UA global optimization method for calibrating watershed models. *J. Hydrol.* 158, 256–284.
- Frind, E.O., Molson, J.W., Schirmer, M., Guiguer, N., 1999. Dissolution and mass transfer of multiple organics under field conditions: the Borden emplaced source. *Water Resour. Res.* 35 (3), 683–694.
- Gorelick, S.M., Evans, B., Remson, I., 1983. Identifying sources of groundwater pollution: an optimization approach. *Water Resour. Res.* 19 (3), 779–790.
- Hatfield, K., Annable, M., Cho, J., Rao, P.S.C., Klammler, H., 2004. A direct passive method for measuring water and contaminant fluxes in porous media. *J. Contam. Hydrol.* 75, 155–181.
- Kapur, J.N., Kesavan, H.K., 1992. *Entropy Optimization Principles with Application*. Academic Press, San Diego.
- Kirkpatrick, S., C.D. Gelatt, J., Vecchi, M.P., 1983. Optimization by simulated annealing. *Science* 220, 671–680.
- Laarhoven, P.J.M.v., Aarts, E.H.L., 1987. *Simulated Annealing: Theory and Applications*. D. Reidel Publishing Company, Dordrecht, Holland. 186 pp.
- Mahar, P.S., Datta, B., 2000. Identification of pollution sources in transient groundwater systems. *Water Resour. Manage. Ser.* 14, 209–227.
- McLaughlin, D., Reid, L.B., Li, S.-G., Hyman, J., 1993. A stochastic method for characterizing groundwater contamination. *Ground Water* 31 (2), 237–249.
- Metropolis, N., Rosenbluth, A.W., Rosenbluth, M.N., Teller, A.H., Teller, E., 1953. Equation of state calculations by fast computing machines. *J. Chem. Phys.* 21 (6), 1087–1092.
- Nelder, J.A., Mead, R., 1965. A simplex method for function minimization. *Comp. J.* 7 (4), 308–313.
- Newman M.A., 2001. *Inverse Characterization of Subsurface Contaminant Mass Flux : A Three-dimensional Physical and Numerical Modeling Study*. Dissertation. University of Florida. Gainesville, Florida.
- Press, W.H., Teukolsky, S.A., Vetterling, W.T., Flannery, B.P., 1992. *Numerical Recipes in FORTRAN: The Art of Scientific Computing*. Cambridge University Press, Cambridge.
- Rao, P.S.C. et al., 2001. Technology integration for contaminant site remediation: cleanup goals and performance criteria. *Groundwater Quality: Natural and Enhanced Restoration of Groundwater Pollution* (Proceedings of the Groundwater Quality 2001 Conference held at Sheffield, UK), IAHS Publication, vol. 275, pp. 571–578.
- Rogers, L.L., Dowl, F.U., Johnson, V.M., 1995. Optimal field-scale groundwater remediation using neural networks and the genetic algorithm. *Environ. Sci. Technol.* 29 (5), 1145–1155.
- Sciortino, A., Harmon, T.C., Yeh, W.W.-G., 2000. Inverse modeling for locating dense nonaqueous pools in groundwater under steady flow conditions. *Water Resour. Res.* 36 (7), 1723–1735.

- Sciortino, A., Harmon, T.C., Yeh, W.W.-G., 2002. Experimental design and model parameter estimation for locating a dissolving dense nonaqueous phase liquid pool in groundwater. *Water Resour. Res.* 38 (5), 15-1–15-10.
- Shore, J.E., Johnson, R.W., 1981. Properties of cross-entropy minimization. *IEEE Trans. Inf. Theory* IT-27 (4), 472–482.
- Sidauruk, P., Cheng, A.H.-D., Ouazar, D., 1998. Groundwater contamination source and transport parameter identification by correlation coefficient optimization. *Ground Water* 36 (2), 208–214.
- Skaggs, T.H., Kabala, Z.J., 1994. Recovering the release history of a groundwater contaminant. *Water Resour. Res.* 30 (1), 71–80.
- Sudicky, E.A., 1989. A natural-gradient experiment on solute transport in a sand aquifer: spatial variability of hydraulic conductivity and its role in the dispersion process. *Water Resour. Res.* 22 (13), 2069–2082.
- Wagner, B.J., 1992. Simultaneous parameter estimation and contaminant source characterization for coupled groundwater flow and contaminant transport modelling. *J. Hydrol.* 135 (1-4), 275–303.
- Wang, P.P., Zheng, C., 1998. An efficient approach for successively perturbed groundwater models. *Adv. Water Resour.* 21 (6), 499–508.
- Woodbury, A., Sudicky, E.A., 1991. The geostatistical characteristics of the Borden aquifer. *Water Resour. Res.* 27 (4), 533–546.
- Woodbury, A.D., Ulrych, T.J., 1993. Minimum relative entropy: forward probabilistic modeling. *Water Resour. Res.* 29 (8), 2847–2860.
- Woodbury, A.D., Ulrych, T.J., 1996. Minimum relative entropy inversion: theory and application to recovering the release history of a groundwater contaminant. *Water Resour. Res.* 32 (9), 2671–2681.
- Woodbury, A.D., Ulrych, T.J., 1998. Minimum relative entropy and probabilistic inversion in groundwater hydrology. *Stoch. Hydrol. Hydraul.* 12, 317–358.
- Woodbury, A., Sudicky, E., Ulrych, T.J., Ludwig, R., 1998. Three-dimensional plume source reconstruction using minimum relative entropy inversion. *J. Contam. Hydrol.* 32 (1-2), 131–158.
- Zheng, C., Wang, P., 1996. Parameter structure identification using tabu search and simulated annealing. *Adv. Water Resour.* 19 (4), 215–224.